Lohmann, P.; Willuweit, A.; Neffe, A.T.; Geisler, S.; Gebauer, T.P.; Beer, S.; Coenen, H.H.; Fischer, H.; Hermanns-Sachweh, B.; Lendlein, A.; Shah, N.J.; Kiessling, F.; Langen, K.-J.:

Bone regeneration induced by a 3D architectured hydrogel in a rat critical-size calvarial defect

In: Biomaterials (2016) Elsevier

DOI: 10.1016/j.biomaterials.2016.10.039

Bone regeneration induced by a 3D architectured hydrogel in a rat critical-size calvarial defect

P. Lohmann[1*], A. Willuweit[1], A.T. Neffe[2], S. Geisler[1], T.P. Gebauer[2], S. Beer[1], H.H. Coenen[1], A. Lendlein[2], N.J. Shah[1], F. Kiessling[3], K.-J. Langen[1]

[1] Institute of Neuroscience and Medicine, Forschungszentrum Jülich, Wilhelm-Johnen-Str., Jülich, 52428, Germany
[2] Institute of Biomaterial Science and Berlin-Brandenburg Center for Regenerative Therapies, Helmholtz-Zentrum Geesthacht, Kantstr. 55, Teltow, 14513, Germany
[3] Institute for Experimental Molecular Imaging, University Clinic and Helmholtz Institute for Biomedical Engineering RWTH Aachen University, Pauwelsstr. 30, Aachen, 52074, Germany

[*] Corresponding Author:
Philipp Lohmann
Institute of Neuroscience and Medicine
Forschungszentrum Jülich
Wilhelm-Johnen-Str.
52428 Jülich
Germany
Fax: +49 2461 61 2302
E-Mail: p.lohmann@fz-juelich.de

Abstract

Bone regeneration can be stimulated by implantation of biomaterials, which is especially important for larger bone defects. Here, the healing potency of the porous ArcGel was evaluated in a critical-size calvarial bone defect in rats in comparison with BioOss® Collagen, which represents a clinical standard material. Fracture healing and metabolic processes involved were monitored longitudinally by [^{18}F]-fluoride and [^{18}F]-FDG µ-PET/CT 1d, 3d, 3w, 6w, and 12w post implantation. Differences in the quality of bone healing were assessed by *ex vivo* µ-CT, mechanical tests and histological stains. Both materials lead to macroscopic healing of the defect, but differences in amount and quality of osteogenesis were identified by µ-CT. More bone was formed after implantation of ArcGel compared with BioOss and the microarchitecture of the new bone was more physiological and better functional (push-out tests). [^{18}F]-FDG uptake increased until 3d after implantation, and then decreased until 12w for both materials. [^{18}F]-fluoride uptake increased until 3w post implantation for both materials, but persisted significantly longer at higher levels for BioOss, which indicates a prolonged remodelling phase. The study demonstrates the potential of ArcGels to induce a *restitutio ad integrum* and better bone regeneration in large defects compared to commercial state-of-the-art biomaterial.

Keywords

Material-induced bone regeneration, regenerative medicine, critical-size calvarial defect, positron-emission-tomography (PET), micro-computed tomography (µ-CT), push-out test

1. Introduction

Bone has the capability under favourable conditions to completely regenerate, e.g. after simple fracture. In contrast, wound healing of tissues of the human body generally leads to the formation of connective tissue, which shows reduced or no function of the original tissue at all [1]. Bone regeneration involves several, partially overlapping phases [2]. In the anabolic phase, cells are recruited to the defect site, a cartilaginous callus is formed, and blood supply is ensured. Following chondrocyte apoptosis, in the catabolic phase cartilage resorption and secondary bone formation occurs. Osteoblast and osteoclast activity are of major importance here and are delicately balanced. Finally, remodelling of the defect site results in regenerated bone. Nevertheless, when the size of a bone defect exceeds a certain size, it will not regenerate spontaneously anymore. Such bone defects are referred to as critical-size bone defects and occur after e.g. severe trauma, primary tumour resection, or infections.

The standard clinical treatment of these critical-size defects is autogenous cancellous bone grafting [3]. In this approach, one implants vital bone including its bone forming cells as well as growth factors to the defect site and avoids rejection of the implant. However, this method has numerous drawbacks such as limited availability of autologous bone, donor site morbidity, pain, and risk of infections [4]. Alternatively, allogenic cancellous bone grafts are used, which may lead to immune or inflammatory response of the host tissue after implantation [5]. Pure biomaterials applied in this context without cells or growth factors used in clinical routine are mainly deproteinised bone matrices [6]. Synthetic materials for this purpose have yet to reach the clinical practice. In addition, cell- and growth factor based strategies, e.g. employing bone morphogenetic proteins, are investigated and applied in the clinics. Reproducibility is a major concern in such cell-based or cytokine-based strategies. These generally are pursued in combination with biomaterials, which ensure an additional mechanical support as well as assist localisation of cells or factors. These combinatory products are challenging from an approval perspective as well as from a producers

perspective. It is not completely clear if all strategies (biomaterials, cells, growth factor, or combinations thereof) under investigation, despite successful bone formation, actually follow a regeneration mechanism similar to the natural regeneration. The status of current concepts and materials for bone healing has recently been summarised in [7, 8].

Ideally, purely biomaterial-based approaches are desirable in terms of production costs, safety, approval process, and availability [9, 10]. However, it still is a challenge to realise an artificial material that overcomes all of the disadvantages mentioned above and shows ideal osteoinductive (stimulation of surrounding cells to start bone formation) and osteoconductive (continuing growth of bone) properties to create new bone and leads to a complete regeneration of a bone defect or fracture. For this purpose, multifunctional materials are required, that display e.g. structural support, allow adhesion, differentiation and proliferation of cells, and are degradable.

Recently, a three-dimensional architectured hydrogel (ArcGel) was introduced consisting of gelatin and lysine connected by urea junction units [11]. This new artificial material led to bone regeneration similar to cancellous bone graft in a critical-size mid-diaphyseal femoral defect in female Sprague Dawley rats. The functions of ArcGels relevant for bone regeneration include display of adhesion sites, a porous architecture enabling cell invasion, and control of the local elasticity.

In this study, a critical-size calvarial defect model in rats [12] was utilised to investigate the bone healing potency and the metabolic processes induced by ArcGel in comparison with the commercial biomaterial BioOss® Collagen (BioOss) (Geistlich Biomaterials, Baden-Baden, Germany) *in vivo*. The course of bone healing was followed by longitudinal X-ray microtomography (µ-CT). While in the earlier work it was shown that ArcGel induced bone regeneration, the underlying metabolic processes such as changes in inflammatory response or osteogenesis during the progression of healing have not yet been investigated. Such processes can be visualised *in vivo* with advanced imaging techniques, which is an important part of this

longitudinal study. Cellular glucose metabolism, which is correlated to the inflammatory response [13], was quantified by positron-emission-tomography (PET) using [^{18}F]-fluorodeoxyglucose ([^{18}F]-FDG). PET imaging of [^{18}F]-fluoride was used to localise regions with high osteoblast activity [14].

BioOss consists of deproteinised bovine spongious bone granules, i.e. hydroxyapatite particles (90 wt.-%) embedded in a spongy-like structure of porcine collagen (10 wt.-%) for enhanced handling characteristics [6, 15]. Multifunctionality of this material is provided through its porous and paste-like structure, which may support cell invasion, as well as the osteoconductivity of the hydroxyapatite component. The collagen is resorbed within a few weeks and is thought not directly to be involved in the process of bone regeneration. This commercially available material was FDA approved in 2004 and used in several preclinical [16, 17] and clinical studies [18, 19], and successfully applied in various oral and maxillofacial indications. The producing company is world market leader for natural bone substitutes in regenerative dentistry [20, 21].

Since the hydroxyapatite particles from BioOss are covering the bone defect and cannot be distinguished from newly formed bone with conventional µ-CT, high-resolution *ex vivo* µ-CT images of the explanted calvaria were acquired at different stages of the study. Additionally, biomechanical push-out tests and histological stains were performed to further evaluate potential differences in the regeneration process induced by the implanted materials.

2. Materials and Methods

2.1 Bone graft materials

ArcGel: 7.5 g of gelatin (Type A, 200 bloom) with low endotoxin content from GELITA AG (Eberbach, Germany) were dissolved in 67.5 ml of water at 48 °C in a flat flange cylindrical jacketed vessel with bottom outlet valve (HWS Labortechnik, Mainz, Germany) under mechanical stirring (500 rpm). Subsequently, 0.75 g PEO-PPO-PEO tri-block copolymer

(Pluronic® F-108, Sigma-Aldrich Chemie, Steinheim, Germany) was added and the mixture stirred at 1500 rpm resulting in the formation of foam. 0.735 ml (3.6 mmol, equivalent to a 3-fold excess of diisocyanate groups compared to amino groups of the gelatin) distilled lysine diisocyanate ethyl ester (LDI) (Chemos GmbH, Regenstauf, Germany) was added under continued stirring, and after 4 min of stirring, the slightly cross-linked foam was collected in cylindrical 100 ml polypropylene beakers and was frozen at -22 °C. After 12 h, frozen samples were given into 600 ml water and washed for 3 d at room temperature to remove unreacted residues. Washed samples were frozen at -18 °C overnight and freeze-dried to achieve dry solid storable scaffolds. Sterilisation was achieved by treatment with 5 vol% ethylene oxide in CO_2.

ArcGels prepared from 10 wt.-% gelatin solutions and a 3-fold excess of isocyanate groups of LDI compared to the amino group content of gelatin (G10_LNCO3) are three-dimensionally structured, elastic recoverable hydrogels, which are cut into the size of the defect in which they are implanted. They display a porosity of 70±8 %, pore sizes of 216±83 µm, and local Young's moduli determined by atomic force microscopy of 1250±140 kPa. The porcine gelatin part offers peptidic cell adhesion sequences. Further details about the properties and synthesis of ArcGel are described in [11].

BioOss: BioOss® Collagen was obtained commercially from Geistlich Biomaterials, Baden-Baden, Germany. As mentioned above, BioOss is deproteinised bovine bone, which contains 10 wt.-% porcine collagen. After addition of water or body fluids, it behaves like a paste, which can be modelled to the site of implantation. The bone granules are 0.25–1.0 mm in size, display a porosity of 75-80 %, a bimodal pore size distribution with macropores of 200-600 µm and micropores < 1 µm, as well as a compressive strength of 35 MPa. As porcine collagen is used, the same types of peptidic cell adhesion sequences are present as in ArcGel. Further details about the properties of BioOss Collagen are provided in [22, 23].

Both materials could be easily adapted to the shape of the bone defect and the handling during implantation was convenient.

2.2 Animal model and surgical procedures

All animal handling and surgical procedures were performed in accordance with the Animal Research: Reporting *In Vivo* Experiments (ARRIVE) guidelines and the German Law on the Protection of Animal and with permit of the local Animal Protection Committee (LANUV NRW Recklinghausen, Germany, no. 84-02.04.2013.A005).

22 male Fischer 344 rats (190-240 g; Charles River Wiga Deutschland GmbH, Sulzfeld, Germany) were used for evaluation of bone regeneration. The animals were housed under standard conditions with *ad libitum* access to food and water.

For bone graft implantation, 18 animals were sedated in a 2 % to 5 % atmosphere of isoflurane and anaesthetised subsequently with an intraperitoneal injection of a mixture of ketamine (100 mg/kg bodyweight) and xylazine (10 mg/kg bodyweight) and were administered tramadol (15 mg/kg bodyweight, subcutaneously) immediately pre-operatively for pain mitigation. A stereotactic frame was used to fix the head and a linear incision was made along the midline of the scalp to expose the cranial bone. An 8 mm diameter calvarial defect was created in the parietal bone, centred over the sagittal suture line between lambda and bregma using a microdrill. The surgical site was continuously rinsed with saline solution to reduce heating. ArcGel was used as sterile discs of 8 mm diameter and 2 mm thickness and soaked in saline solution prior to implantation into the defect (n = 9). BioOss was soaked in saline solution, moulded to discs of similar size (8 mm diameter, 2 mm thickness) and carefully placed into the bone defect (n = 9) before the wound was sutured.

2.3 Longitudinal PET/µ-CT measurements

16 animals with implanted bone grafts (ArcGel n = 8, BioOss n = 8) underwent dynamic, longitudinal PET/µ-CT measurements (Siemens INVEON, Siemens Healthcare, Erlangen, Germany) at different time points post implantation (1 d, 3 d, 3 w, 6 w, 12 w).

The animals were anaesthetised in a 2 % atmosphere of isoflurane. A bolus injection of approximately 50 MBq [^{18}F]-FDG (Group 1: ArcGel n = 4, BioOss n = 4) or [^{18}F]-fluoride (Group 2: ArcGel n = 4, BioOss n = 4) dissolved in 500 µl saline solution was administered intravenously into the tail vein via a catheter. Group 1 was fasted 12 h before the [^{18}F]-FDG PET examination. All animals remained anaesthetised and heated after tracer application, hereby reducing the uptake of [^{18}F]-FDG in brown fat tissue in the neck region of the animals, to minimise the background signal. *Ad libitum* access to water was provided.

The animals were positioned in the µ-CT (head first prone) with the bone defect centred in the field-of-view (FOV) for evaluation of fracture healing. The X-ray source voltage was set to 80 kVp and the anode current to 500 µA. The image data (Image matrix 480 x 480 x 636) were reconstructed using a modified Feldkamp algorithm resulting in a reconstructed voxel size of 0.2 mm^3. The total scan time was 05:18 min.

The amount of newly formed bone after implantation of ArcGel was determined using the open-source image processing applications OsiriX 6.1 [24] and Fiji 2.0.0-rc-9 [25]. Two-dimensional transversal views from three-dimensional reconstructions of the µ-CT images were used. The images were converted into binary images and the extent of the bone defect was determined using an auto-contouring algorithm. The size of the original defect S_0 was evaluated in the µ-CT image 24 h post implantation.

The amount bone covering the initial defect post implantation of ArcGel was calculated by (1-S_x/S_0), where S_x represents the size of the defect at time x post implantation. This method could not be used for evaluation of BioOss, because the hydroxyapatite particles from BioOss inside the defect cannot be distinguished from newly formed bone with conventional µ-CT.

Here, the course of bone healing was qualitatively evaluated by visual analysis of the acquired µ-CT images.

After CT acquisition, dynamic PET emission data were acquired in list mode format from 60 to 75 min post injection (p.i.) (3 x 5 min frames). The attenuation map for attenuation correction was generated from the µ-CT image. The image data were also corrected for decay, random and scatter coincidences, and dead time prior to reconstruction using a fast maximum *a posteriori* (FastMAP) algorithm in conjunction with a 3D ordered-subset expectation maximisation algorithm (OSEM-3D) with two OSEM-3D iterations and 18 MAP iterations resulting in a reconstructed voxel size of 0.8 mm^3 (Image matrix 128x128x159). Averaged PET images (60-75 min p.i.) and the corresponding µ-CT images were imported into PMOD (Version 3.5, PMOD Technologies Ltd., Zuerich, Switzerland). Since the images were acquired sequentially without changing the position of the animal, no co-registration was necessary. If slight mismatches in co-registration due to motion of the animal during the measurement were observed, manual co-registration was performed. The total injected activity was corrected for decay and the uptake of [^{18}F]-FDG or [^{18}F]-fluoride was expressed as injected dose per millilitre tissue. The values were normalised to an injected dose of 50 MBq. Three-dimensional volumes-of-interest (VOI) were used for analysis. A 10 x 10 x 3 mm^3 (length x width x height) VOI was defined in the µ-CT image (centred in the calvarial defect) and applied to the co-registered PET image. The mean uptake values for each animal and tracer were analysed and compared. Metabolic differences induced by the two materials during the process of bone healing were statistically evaluated using the software InVivoStat [26]. Descriptive statistics are provided as mean and SD. To investigate the longitudinal effects of the implanted materials with respect to the processes involved in bone healing, two way repeated measure ANOVA with appropriate *post hoc* tests were performed. P-values of less than 0.05 were considered statistically significant.

2.4 Sample preparation

All animals were sacrificed by decapitation under deep isoflurane sedation. 16 animals that were included in the longitudinal PET/µ-CT measurements were sacrificed 1 d after the last PET/µ-CT measurement (12 weeks post implantation). Two animals (ArcGel n = 1, BioOss n = 1) were sacrificed 7 w after implantation.

The parietal bone was extracted and remaining soft tissue was carefully removed. The inner part of the calvaria was visually inspected for complete (no visible holes) or incomplete (visible holes) healing of the defect. The samples were stored at -20 °C for further processing.

2.5 High-resolution ex vivo µ-CT

High-resolution *ex vivo* µ-CT images of the explanted parietal bone were acquired (Skyscan 1172, Bruker, Billerica, MA, USA) from one representative animal for each substrate at 7 w (ArcGel n = 1, BioOss n = 1) and 12 w (ArcGel (n = 1), BioOss (n = 1)) after implantation. The X-ray source voltage was set to 59 kV and the anode current to 167 µA. The image data were reconstructed using a vendor provided high-speed volumetric reconstruction software resulting in a reconstructed pixel size of about 4.0 µm. The total scan time was 80 min. The acquired images were visually inspected using the software CTvox (Version 3.0, Bruker, Billerica, MA, USA) for differences in fracture healing.

2.6 Mechanical testing

A destructive push-out test was performed to evaluate the mechanical properties of the explanted parietal bone 12 w post implantation (ArcGel n = 4, BioOss n = 4). Parietal bone samples without any bone defect from male Fischer F344 rats were used to obtain a reference value for healthy bone (Control n = 4).

A 5 mm diameter push-out jig was centred in the defect site, with the inner surface of the explanted bone facing towards the jig. The push-out jig was moved at a constant speed

(0.6 mm/s) and the force until failure and the corresponding position was measured (Load cell: U9C, HBM, Darmstadt, Germany; displacement sensor: LAS-T-100, WayCon, Bruehl, Germany).

The acquired data were normalised to the sample thickness and the corresponding load-displacement diagrams were visually analysed. The maximum load for each sample was evaluated and the mean push-out strengths were compared. Slopes of the load-displacement curves before failure as a measure of elasticity or ductility were evaluated using a linear fit. The descriptive statistics are provided as mean and SD. To compare the differences of the mean push-out strengths and the mean slope of the different samples, the one-way ANOVA with Bonferroni *post hoc* was used. P-values of less than 0.05 were considered statistically significant. Statistical analyses were performed using SPSS statistics software (IBM SPSS Statistics Version 21, IBM Corp., Armonk, NY, USA).

2.7 Safranin O staining

Four samples intended for use in histology (ArcGel n = 2, BioOss n = 2) were embedded in cold optimal cutting temperature compound (OCT) without prior fixation. Cryosections of 20 µm thickness were prepared using a cryomicrotome (CM3050, Leica Microsystems GmbH, Wetzlar, Germany). The bone samples were not decalcified prior to cutting, thus, special disposable blades for dense samples (Surgipath DB80 LX, Leica Biosystems, Nussloch, Germany) were used. The cryosections were histologically stained using a Safranin O staining protocol. This staining is frequently used in bone research and is recommended for the visualisation and detection of cartilage, mucin, and mast cell granules. The cartilage and mucin will be stained orange to red, and the nuclei will be stained black. The background is stained bluish green.

After staining, the results were analysed using a stereo microscope (LMD6500, Leica Microsystems GmbH, Wetzlar, Germany). The vendor provided software was used for visual

analysis of the acquired images (Leica Application Suite, Leica Microsystems GmbH, Wetzlar, Germany).

Results

3.1 Longitudinal PET/µ-CT measurements

No bone formation was observed until 3 d post implantation of ArcGel. The amount of bone formed 3 w after implantation of ArcGel was covering 78±23 % of the initial defect and slightly increased to 79±19 % after 6 w. The bone defect was completely closed after 12 w in 5 animals and bone was formed covering between 82 % to 98 % of the initial defect in 3 animals, i.e. 95±7 % of the initial defect was covered by newly formed bone 12 w after implantation of ArcGel.

The healing, i.e. the osteogenic potential of BioOss could not be evaluated with this method, because the hydroxyapatite particles inside the defect cannot be distinguished from endogenous bone with conventional µ-CT. Nevertheless, the bone defect was also macroscopically closed after 12 w. Radiographic images (sagittal and coronal slices) of the healing process over time of representative animals are shown in Fig. 1.

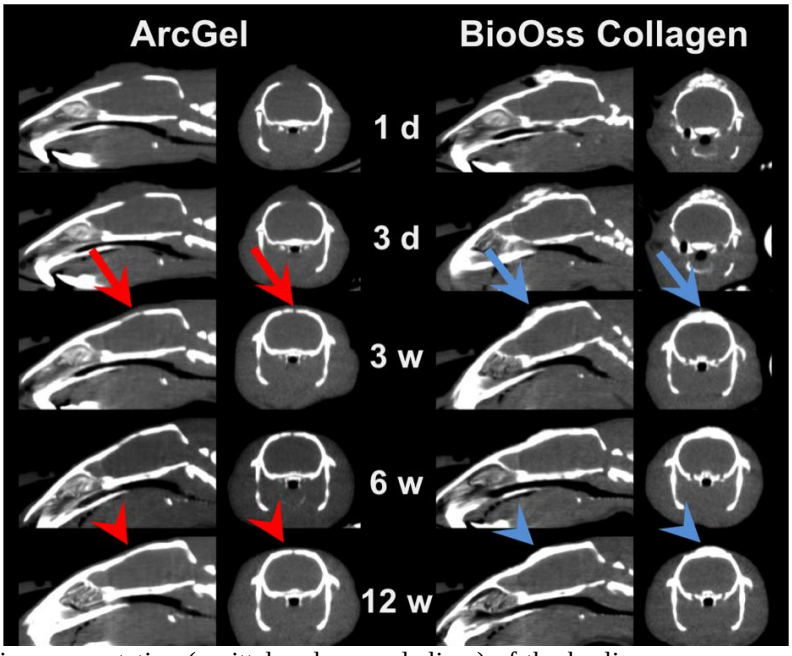

Fig. 1: Radiographic representation (sagittal and coronal slices) of the healing process over time. Images were acquired longitudinally at 1 d, 3 d, 3 w, 6 w and 12 w post implantation of ArcGel (left column) and BioOss (right column) into the critical-size defect. An osseous flap was formed already 3 w after implantation of ArcGel (red arrow, left column), whereas the defect was covered and filled with the implant material BioOss itself (blue arrow, right column). Closing of the defect was observed for both materials 12 w after implantation (arrowheads).

All animals showed an increased uptake of [^{18}F]-FDG in the area of the defect in the early phase after implantation (1 d post implantation: ArcGel: 1.02±0.36 %ID/ml, BioOss: 0.98±0.07 %ID/ml; 3 d post implantation: ArcGel: 0.89±0.11 %ID/ml, BioOss: 0.87±0.26 %ID/ml), which continuously decreased until 12 w post implantation (ArcGel: 0.48±0.05 %ID/ml, BioOss: 0.58±0.06 %ID/ml).

The uptake of ^{18}F-fluoride 1 d after implantation was 0.78±0.2 %ID/ml for ArcGel and 0.76±0.11 %ID/ml for BioOss. The maximum uptake of ^{18}F-fluoride was observed 3 d after implantation for both materials (ArcGel: 1.50±0.12 %ID/ml (n = 3), BioOss: 1.50±0.35 %ID/ml) and remained on an increased level until 3 w after implantation (ArcGel: 1.33±0.36 %ID/ml (n = 3), BioOss: 1.16±0.03 %ID/ml (n = 3)) (Fig. 2). The uptake of [^{18}F]-fluoride 12 w post implantation of ArcGel decreased to 0.71±0.07 %ID/ml, whereas it persisted significantly longer for BioOss (1.08±0.25 %ID/ml (n = 3), p = 0.027).

PET/µ-CT images of representative animals 3 w after implantation of ArcGel and BioOss are shown in Fig. 2 and the results are summarised in Fig. 3.

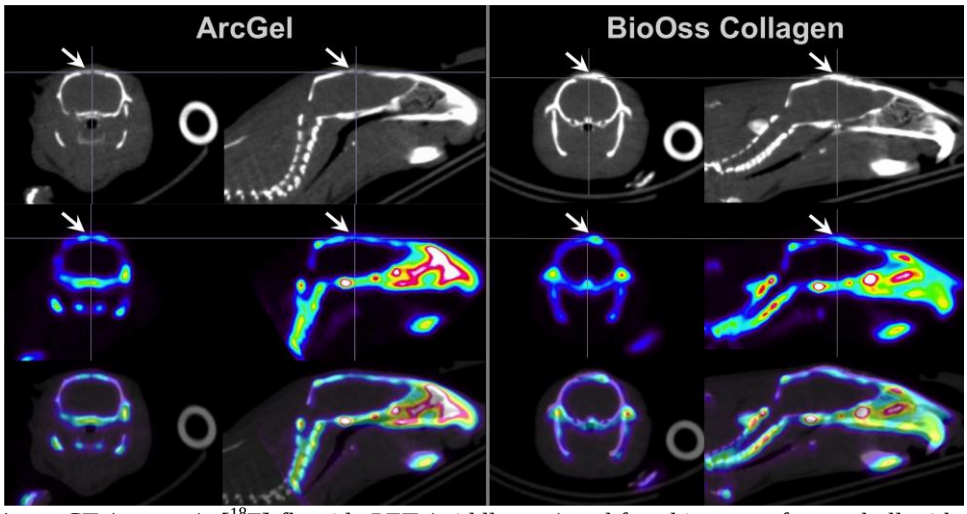

Fig. 2: *In vivo* µ-CT (top row), [^{18}F]-fluoride PET (middle row) and fused images of a rat skull with critical-size calvarial defect 3 w post implantation of ArcGel (left) and BioOss (right) in coronal and sagittal slices. Enhanced uptake of [^{18}F]-fluoride in the area of the bone defect (white arrow) was observed.

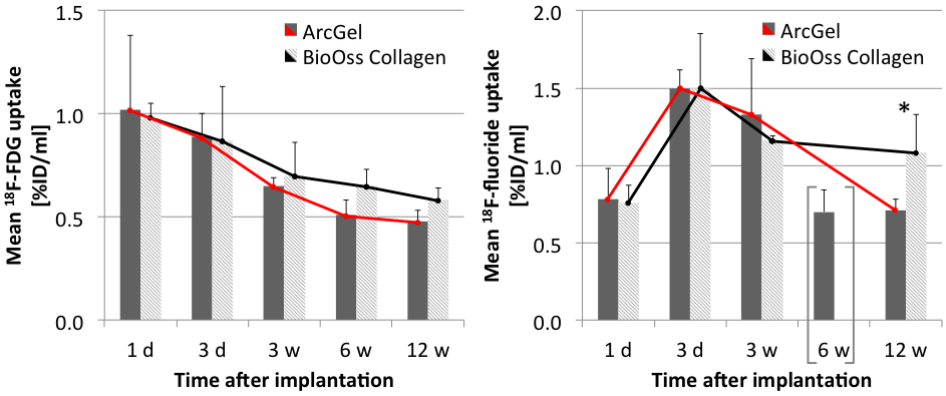

Fig. 3: Mean uptake of [^{18}F]-FDG (left) and [^{18}F]-fluoride (right) over the course of the longitudinal study. All animals showed an increased uptake of [^{18}F]-FDG in the area of the defect in the early phase after implantation, which continuously decreased until 12 w post implantation. The maximum uptake of [^{18}F]-fluoride was observed 3 d after implantation for both materials and remained on an increased level until 3 w after implantation. The uptake of [^{18}F]-fluoride 12 w post implantation for BioOss persisted significantly longer compared to ArcGel (* $p = 0.027$). The time point 6 w post implantation could only be acquired for ArcGel due to technical problems during tracer synthesis and was excluded from the statistical analysis.

Three ^{18}F-fluoride PET measurements were available for inclusion in this study at time point 3 d after implantation (ArcGel), 3 w after implantation (ArcGel, BioOss) and 12 w after implantation (BioOss) as indicated above, because of technical reasons. The ^{18}F-fluoride PET measurements for BioOss 6 w post implantation could not be performed due to irregularities in tracer production. Thus, this time point was completely rejected from the statistical evaluation, but is still included in the graphical representation of the results in Fig. 3.

3.2 Visual inspection of the samples and high-resolution ex vivo µ-CT

Visual inspection of the explanted parietal bone showed a complete macroscopic healing of the calvarial defect at the end of the observation period after 12 weeks for both materials (Fig. 4).

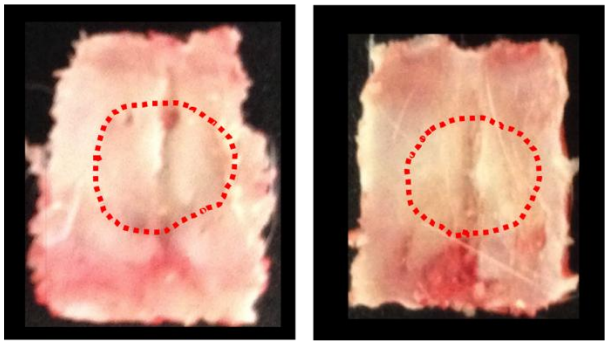

Fig. 4: Photograph of explanted calvaria (inner side) from representative animals 12 w after implantation of ArcGel (left) and BioOss (right). Complete macroscopic healing of the original critical-size bone defect (indicated by red dashed line) was observed in all animals

However, the analysis of the high resolution *ex vivo* µ-CT images revealed differences between the two materials (Fig. 5). The calvarial defect was nearly completely covered by a bony flap 7 w after implantation of ArcGel (Fig. 5, A1-A2). Although, the defect was nearly closed, the newly formed bone appeared less dense, i.e. not fully calcified and thinner than the original parietal bone (Fig. 5, A3). 12 w after implantation of ArcGel, the defect was closed (Fig. 5, C1-C2) and both the level of calcification and the thickness of the newly formed bone were similar to the original parietal bone (Fig. 5, C3).

In the case of BioOss implantation, the calvarial defect was macroscopically closed after 7 w (Fig. 5, B1-B2). However, the defect was basically covered and filled up with hydroxyapatite particles from the original implant. These particles appeared as sharply demarcated hyperdense fragments in the *ex vivo* µ-CT (Fig. 5, B3) compared to the small amount of newly formed bone in the area of the defect that showed lower density. The amount of newly formed bone slightly increased 12 w after implantation of BioOss (Fig. 5, D1-D3), but was not covering the whole defect and the amount of newly formed bone appeared to be considerably less than after implantation of ArcGel. The hydroxyapatite particles were still

covering the defect, but were more densely packed and remodelled to better reflect the original shape of the parietal bone (Fig. 5, D3). There was still surplus implant material covering the defect clearly different from the original shape and thickness of the physiological calvaria.

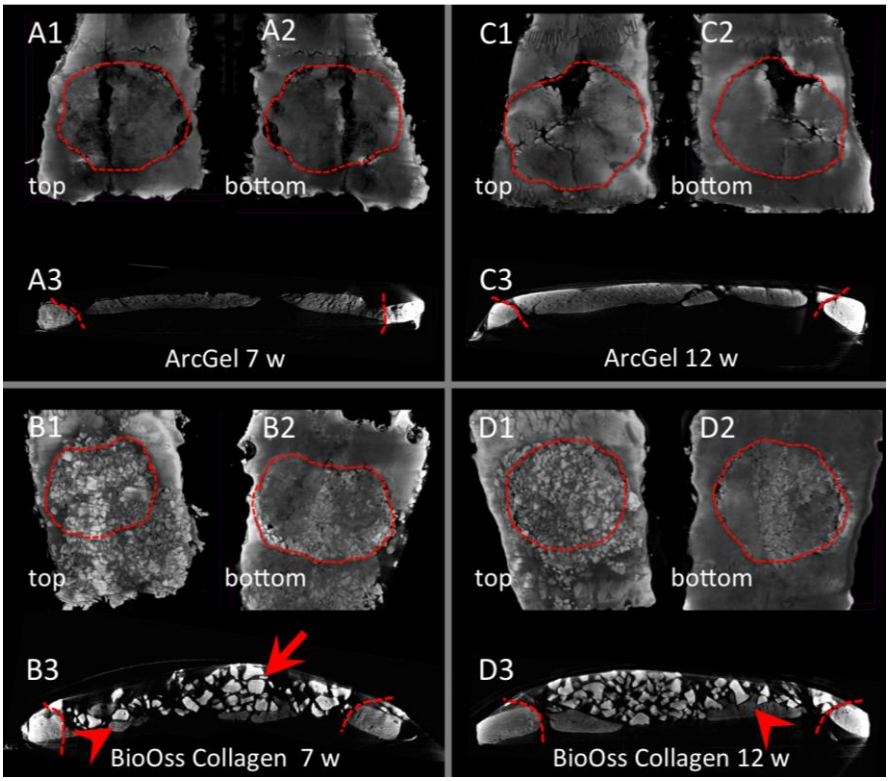

Fig. 5: Three-dimensional (1, 2) and cross-sectional (3) images of high resolution *ex vivo* µ-CT scans of the explanted calvaria 7 w (A, B) and 12 w (C, D) post implantation of ArcGel (top row) and BioOss (bottom row). The original bone defect (indicated by the red dashed line) was nearly completely covered by a bony flap 7 w after implantation of ArcGel (A1-A2), but the newly formed bone appeared less dense, i.e. not fully calcified and thinner than the original parietal bone (A3). 12 w after implantation of ArcGel, the defect was closed (C1-C2) and both the level of calcification and the thickness of the newly formed bone were similar to the original parietal bone (C3). The missing bone fragment in C1-C2 unfortunately broke out during sample preparation. The defect was also closed 7 w after implantation of BioOss (B1-B2). The defect was filled with hydroxyapatite particles from the original implant, that appear as sharply demarcated hyperdense fragments (B3, arrow) compared to the small amount of newly formed bone in the area of the defect that showed lower density (B3, arrowhead). The amount of newly formed bone slightly increased 12 w after implantation of BioOss (D1-D3, arrowhead). Although both materials lead to a macroscopic healing of the defect, only ArcGel induced complete healing also on a microscopic scale.

3.3 Mechanical testing

The load-displacement curves (Fig. 6) of the healthy bone samples showed a steep increase (average slope 5.83±0.75) until failure of the sample at maximum load, followed by an instantaneous drop. A very similar curve pattern was also observed after implantation of ArcGel. The average slope of the load displacement curve during the loading phase was 3.84±1.17 followed by the same instantaneous drop. The BioOss samples showed a flatter increase of load until failure (average slope 1.24±0.69) and no instantaneous drop afterwards, but a slow decrease of load. The differences in average slope were statistically significant (ArcGel vs. BioOss, BioOss vs. Control ($p < 0.01$); ArcGel vs. Control ($p < 0.05$) and are summarised in Fig. 7, right.

The mean push-out strengths were 4.33±1.32 MPa for ArcGel, 1.47±0.42 MPa for BioOss and 7.91±1.46 MPa for the control group (Fig. 7, left). These differences in push-out strengths were statistically significant (ArcGel vs. BioOss ($p < 0.05$); ArcGel vs. Control, BioOss vs. Control ($p < 0.01$). The results are summarised in Fig. 7, left.

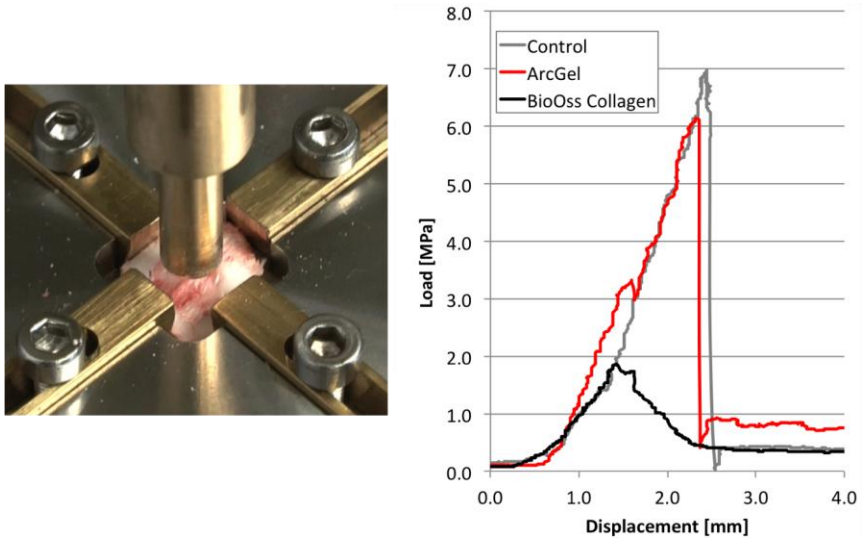

Fig. 6: Mechanical push-out tests were performed with a 5 mm diameter jig (left) until failure of the sample. Representative load-displacement curves (right) showed a typical pattern for healthy control, i.e. a steep increase followed by an instantaneous drop after failure (grey). A similar pattern was also observed for ArcGel (red), whereas BioOss (black) showed a slow increase and also a slow decrease after failure.

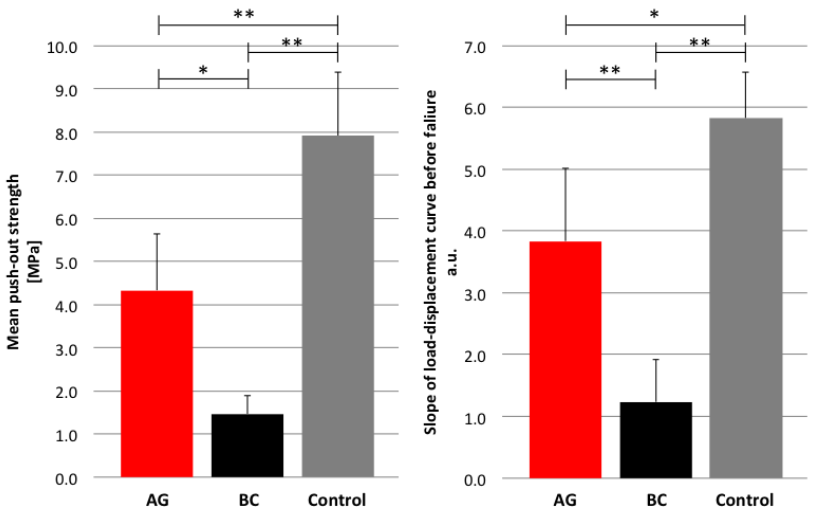

Fig. 7: Mean push-out strength (left) and slope of load-displacement curve before failure (right) as measured with the push-out test. The mean push-out strength for ArcGel was significantly higher than for BioOss. The mean slope of the load-displacement curve was significantly higher for ArcGel than BioOss. (* $p < 0.05$, ** $p < 0.01$)

3.4 Safranin O staining

Safranin O staining of the explanted parietal bone 12 w after implantation of ArcGel (Fig. 8, top row) showed the formation of new bone in the defect. The original bone appeared dark green, while the newly formed bone appeared brighter and less dense. Further magnification showed the presence of bone cells in the area of the newly formed bone. No cartilage and no residuals of the original implant could be observed.

In the defects filled with BioOss, newly formed bone was observed and the hydroxyapatite particles from the original implant were distributed over the entire grafted area (Fig. 8, bottom row). Also here, the original parietal bone appeared dark green, while the newly formed bone was brighter and less dense. The hydroxyapatite particles of the original implant are stained purple or red, which indicates the presence of a thin layer of cartilage around the particles. The formation of new bone seemed to originate from the surface of the hydroxyapatite particles. Further magnification also showed the presence of bone cells in the area of the newly formed bone.

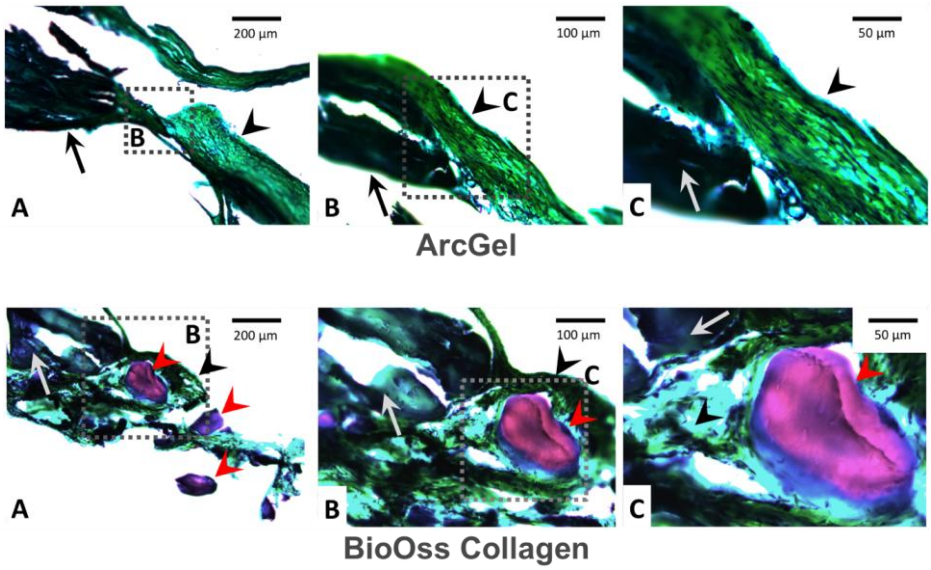

Fig. 8: Cross section of explanted calvaria 12 w after implantation of ArcGel (top row, A 10x, B 20x, C 40x magnification) and BioOss (bottom row) after histological Safranin O staining. The original parietal bone appeared dark green (arrow) after implantation of ArcGel, while the newly formed bone was brighter and less dense (arrowhead). Further magnification showed bone cells in the area of the newly formed bone. No residuals of the original implant could be observed. After implantation of BioOss (bottom row, A 10x, B 20x, C 40x), the original parietal bone appeared dark green (white arrow), while the newly formed bone was brighter and less dense (black arrowhead). The hydroxyapatite particles from the original implant (red arrowhead) are stained purple to red, which indicates the presence of a thin layer of cartilage around the particles. The formation of new bone seemed to originate from the surface of these particles.

Discussion

The main goal of this study was to evaluate the osteogenic potency of ArcGel compared to a widely used commercial bone graft material BioOss in a critical-size calvarial defect model in rats, whereby metabolic, functional and morphological parameters were evaluated using longitudinal small animal PET/µ-CT imaging. Furthermore, to gain a better understanding of the healing process and quality, additional *in vivo* and *ex vivo* µ-CT measurements, mechanical tests and histological stains were performed.

All results obtained with ArcGel were compared with a second, commercially available bone graft material BioOss in order to better classify the results and identify potential differences in the healing approach between the materials.

The mechanisms of bone regeneration induced by the two investigated materials are thought to be quite different, though both display a porous structure and provide cell adhesion sequences such as RGD and GFOGR in their gelatin/collagen part. The functionality of

ArcGels was explained by supporting cell differentiation by control of local elasticity [11], a phenomenon first described in stem cell culture [27], as well as by mechanical stimulation of cells by pore growth during the degradation phase. The relatively fast degradation with pore size growth is furthermore thought to provide space to growing tissue as well as for the calcification. The osteoconductivity of hydroxyapatite-based materials such as BioOss in contrast has been related to their dissolution and the effect of dissolved calcium and phosphate ions in the defect site [28].

The calvarial defect model in rats for evaluation of the healing properties of bone graft materials was already used in several studies [4, 12, 29, 30] and a diameter of 5 to 8 mm was described as critical-size in rats [31, 32]. Therefore, a defect at the upper limit of this range of 8 mm diameter was used to ensure a critical-size defect.

PET imaging using the tracers [^{18}F]-FDG and [^{18}F]-fluoride for measuring inflammatory responses to the implanted material and osteogenesis, respectively, was used before for the preclinical assessment of fracture healing in several studies [14, 33, 34]. In a comparative [^{18}F]-FDG PET study of osteomyelitis and normal bone healing in rabbits, normal bone healing was associated with an increased uptake of [^{18}F]-FDG in the early phase which normalised within six weeks [35].

In this study, an increased uptake [^{18}F]-FDG was observed in the early phase after implantation (1 – 3 d), which continuously decreased until 12 w for both materials. Presumably, the initial inflammatory response to the surgical intervention is responsible for the increased uptake of [^{18}F]-FDG in the early phase rather than a response related to the implanted materials. The use of Tramadol as analgesic, which does not provide anti-inflammatory effects, the steady decrease of [^{18}F]-FDG uptake until 12 w after implantation, and the lack of significant differences between the two materials also supports this interpretation. An earlier *in vitro* study about the biocompatibility of gelatin crosslinked with LDI in the form of films investigated the expression of the pro-inflammatory proteins

cyclooxygenase-1 (COX-1), cyclooxygenase-1 (COX-2), and the receptor for advanced glycation endproducts (RAGE) via Western blotting. The influence of these degradation products was studied in cells that were cultivated with eluates of ArcGel films after incubation in trypsin or buffer solution. No signs of an acute inflammatory response could be observed *in vitro* and *in vivo* [36].

The uptake of [^{18}F]-fluoride was increased already 3 d after implantation and remained at this level until 3 w after implantation for both materials. While the uptake of [^{18}F]-fluoride of ArcGel decreased until 12 w post implantation, it remained significantly higher for BioOss until the end of the observation period. This increased uptake indicates a prolonged phase or slower bone remodelling induced by BioOss compared to ArcGel.

BioOss was described as participating in the remodelling process [37]. The hydroxyapatite particles of BioOss serve as starting points for bone formation, which was also observed after histological Safranin O staining. The complete remodelling after implantation of BioOss takes several months to years to be fully completed [37]. This prolonged period of remodelling probably leads to the longer persisting uptake of [^{18}F]-fluoride measured for BioOss.

In contrast, ArcGel showed a decreasing osteogenic activity from 3 w until 12 w post implantation. ArcGel is completely resorbed within a few weeks [11], which was confirmed by the lack of residuals of ArcGel in the histological evaluation after Safranin O staining. Already 3 w after implantation of ArcGel, an osseous flap started to form and covered 78±23 % of the critical-size calvarial defect. Complete regeneration of the defect was achieved 12 w after implantation with a bony coverage of 95±7 %.

These results are supported by the findings from the *ex vivo* µ-CT measurements. The amount of newly formed bone 7 w and 12 w after implantation was small for BioOss compared to ArcGel. The hydroxyapatite particles of the implant (BioOss) were incorporated into a small amount of newly formed bone, which is due to the mechanism of action of BioOss mentioned above. Thus, BioOss acts as an osteoconductive material.

The push-out tests confirmed the results from the *ex vivo* µ-CT images. A larger amount of bone is formed in the case of ArcGel that leads to a statistically significant increased mean push-out strength compared to BioOss. Besides the amount, also the quality of bone formed by ArcGel was very similar to physiological bone. The shape of the load displacement curves [38] for ArcGel showed a comparable pattern as the healthy control samples, which is a typical curve pattern for a brittle fracture.

On the other hand, the slower decrease of load after failure of BioOss is typical for a more elastic or ductile fracture behaviour. This is probably due to the smaller amount of newly formed bone in the defect site after the end of the observation period. Since the process of complete fracture healing and integration of the implant into endogenous bone is slower with BioOss, the quality of the bone is not comparable to physiological bone at this stage of fracture healing.

These results suggest that ArcGel led to bone regeneration similar to endogenous repair processes during osteogenesis as the tissue cannot be distinguished from the original body´s own tissue. The fast degradation of the material reduces the risk of long-term detrimental effects such as inflammatory or immunogenic responses of the body against the implant. Such natural regeneration is mentioned as one of the final goals of regenerative medicine [39]. It is remarkable, that ArcGel induces a *restitutio ad integrum*[1] as material without the addition of cells, growth factors, or surface coatings [3, 7, 30], which is commonly done in other approaches to guide the cell differentiation and bone regeneration. This, however, fits to the hypothesis that as an osteoinductive material ArcGel initiates a natural regeneration cascade. In alternative approaches, growth factors have to be delivered in high concentrations to overcome the short biological half-life and to ensure a sufficient level to be sensed by the target tissue. However, high doses of growth factors can cause severe side effects, such as pathological vessel formation and even tumour growth [40, 41]. Thus, the controlled release

[1] Restoration to original or uninjured condition

of growth factors attached to bone graft materials is still under investigation and, obviously, a growth factor free approach is preferred.

A further point of interest is to highlight similarities and differences between the studied materials and the way they induce bone formation here in order to explore reasons for the different performance of ArcGel and BioOss in this study. While both materials contain porcine collagen or its derivative gelatin, and therefore display the same type of peptidic cell adhesion sequences, the organic matrix content of ArcGel is much higher than of BioOss, so it is likely that there are more cell adhesion sequences available in ArcGel than in BioOss. The cell adhesion sequences are important for initial cell settling, but also motility of cells [42] within a porous structure, so that cells might more readily invade ArcGel than BioOss. The local mechanics of the materials, which play an important role in cell differentiation and proliferation, differ strongly, with ArcGel being a much softer material. This highlights the point that during bone growth and regeneration, guiding materials might actually not have to display mechanical properties of the final bone. The elasticity of ArcGel together with the cell attachment points and growing pores over time might contribute to the regeneration through mechanical stimulation of cells, which cannot be provided by BioOss, as the bone granules are rigid. While the bioactivity of hydroxyapatite-based materials is ruled by their dissolution, the mineral part of BioOss collagen was actually very slowly, if at all during the observed time frame, dissolving, but was rather incorporated into the defect site. This may be interpreted as a wound healing process with incorporation of a body foreign material rather than bone regeneration as in the case of ArcGel, and could explain the differences in the mechanical performance of the defect sites 12 w after implantation. The remodelling after implantation of ArcGel might actually be supported by the growing pores during degradation, which subsequently allow vascularisation. This shows a potential benefit of the relatively fast degradation rate of ArcGel.

Conclusions

The investigated bone graft materials differed in their properties and the biological mechanisms that were induced by the biomaterials that finally led to bone healing. Whereas BioOss acts as a osteoconductive material, using hydroxyapatite particles as starting point for long-term bone formation, ArcGel acts as a highly osteoinductive material. The largest differences of the two studied materials concerns the hypothesised mechanisms of bone regeneration, with the data supporting ArcGel to act as a material supporting the native bone regeneration process, while the BioOss dissolution being too slow to enable an effective remodelling process, so that here a wound healing process is occurring. The combination of properties for ArcGel seems more favourable for inducing a *restitutio ad integrum* than for BioOss. Although both materials led to a closing of the defect, only ArcGel induced a complete regeneration of the bone defect. The newly formed bone could hardly be distinguished from the body´s own bone and also the mechanical properties were very similar to healthy bone already after 12 w of healing.

Thus, ArcGel seems to be a very promising bone graft material for functional regeneration of critical-size bone defects, which would distinguish it from the current clinical standard for treatment of critical-size bone defects, the autogenous cancellous bone graft, which has limited availability and associated risks. The preclinical and clinical evaluation of ArcGel will be continued.

Acknowledgements

The authors thank the Helmholtz Association for funding of this work through Helmholtz-Portfolio Topic “Technologie und Medizin – Multimodale Bildgebung zur Aufklärung des In-vivo-Verhaltens von polymeren Biomaterialien”; and Markus Lang, Christoph Mülder, Werner Lesmeister, Steffen Wolf, Dr. Harald Glückler, Angela Weißhaupt, and Andrea Radermacher for their support and technical assistance.

Especially, the technical help and overall support of Nicole Niemietz and Michael Schöneck is greatly acknowledged.

References

1 Hing KA. Bone repair in the twenty-first century: biology, chemistry or engineering? Phil Trans R Soc Lond A 2004;362:2821-50.

2 Einhorn TA, Gerstenfeld LC. Fracture healing: mechanisms and interventions. Nat Rev Rheumatol 2015;11:45-54.

3 Lichte P, Pape HC, Pufe T, Kobbe P, Fischer H. Scaffolds for bone healing: Concepts, materials and evidence. Injury, Int J Care Injured 2011;42:569-73.

4 Szpalski C, Barr J, Wetterau M, Saadeh PB, Warren SM. Cranial bone defects: current and future strategies. Neurosurg Focus 2010;29(6):1-11.

5 Gazdag AR, Lane JM, Glaser D, Forster RA. Alternatives to Autogenous Bone Graft: Efficacy and Indications. J Am Acad Orthop Surg 1995;3:1-8.

6 Trevisiol L, Nocini PF, Albanese M, Sbarbati A, D´Agostini A. Grafting of Large Mandibular Advancement With a Collagen-Coated Bovine Bone (Bio-Oss Collagen) in Orthognatic Surgery. J Craniofac Surg 2012;23(5):1343-48.

7 Dimitriou R, Jones E, McGonagle D, Giannoudis PV. Bone regeneration: current concepts and future directions. BMC Medicine 2011;9:66.

8 Schroeder JE, Mosheiff R. Tissue engineering approaches for bone repair: Concepts and evidence. Injury, Int J Care Injured 2011;42:609-13.

9 Myeroff C, Archdeacon, M. Autogenous bone graft: donor site and techniques. J Bone Joint Surg Am 2011;93(23):2227-36.

10 Heneghan HM, McCabe JP. Use of autologous bone graft in anterior cervical decompression: morbidity & quality of life analysis. BMC Musculoskeletal Disorders 2009;10:158.

11 Neffe A, Pierce BF, Tronci G, Ma N, Pittermann E, Gebauer T, et al. One Step Creation of Multifuntional 3D Architectured Hydrogels Inducing Bone Regeneration. Adv Mater 2015;27:1738-44.

12 Spicer PP, Kretlow JD, Young S, Jansen JA, Kasper FK, Mikos AG. Evaluation of bone regeneration using the rat critical size calvarial defect. Nat Protoc 2012;7(10):1918-29.

13 Love C, Tomas MB, Tronco GG, Palestro CJ. FDG PET of infection and inflammation. Radiographics 2005;25(5):1357-68.

14 Hsu WK, Feeley BT, Krenek L, Stout DB, Chatziioannou AF, Lieberman JR. The use of ^{18}F-fluoride and ^{18}F-FDG PET scans to assess fracture healing in a rat femur model. Eur J Nucl Med Mol Imaging 2007;34:1291-301.

15 Rohner D, Hailemariam S, Hammer B. Le Fort I osteotomies using Bio-Oss® Coallagen to promote bony union: a prospective clinical split-mouth study. Int J Oral Maxillofac Surg 2013;42(5):585-91.

16 Jung U-W, Lee J-S, Lee G, Lee, I-K, Hwang J-W, Kim M-S, et al. Role of collagen membrane in lateral onlay grafting with bovine hydroxyapatite incorporated with collagen matrix in dogs. J Periodontal Implant Sci 2013;43(2):64–71.

17 Wong RWK, Rabie ABM. Effect of Bio-Oss® Collagen and Collagen Matrix on Bone Formation. The Open Biomed J 2010;4:71-6.

18 Cardaropoli D, Tamagnone L, Roffredo A, Gaveglio L, Cardaropoli G. Socket preservation using bovine bone mineral and collagen membrane: a randomized controlled clinical trial with histologic analysis. Int J Periodontics Restorative Dent 2012;32(4):421-30.

19 Jung RE, Philipp A, Annen BM, Signorelli L, Thoma DS, Hämmerle CHF, et al. Radiographic evaluation of different techniques for ridge preservation after tooth

extraction: a randomized controlled clinical trial. J Clin Periodontol 2013;40(1):90-8.

20 iData Research Inc., US Dental Bone Graft Substitutes and other Biomaterials Market, 2011.

21 iData Research Inc., European Dental Bone Graft Substitutes and other Biomaterials Market, 2012.

22 Li S-T, Chen H-C, Pierson D, Yuen D, Hansen P. NuOss®, a Bone Grafting Material for Oral Surgery: A Comparative Study with BioOss. Collagen Matrix Inc., Franklin Lakes, NJ 07417 USA.

23 Sollazzo V, Palmieri A, Scapoli L, Martinelli M, Girardi A, Alviano F, Pellati A, Perrotti V, Carinci F. Bio-Oss® acts on Stem cells derived from Peripheral Blood. Oman Med J 2010;25(1):26-31.

24 Rosset A, Spadol L, Ratib O. OsiriX: An Open-Source Software for Navigating in Multidimensional DICOM Images. J Digit Imaging 2004;17(3):205-16.

25 Schindelin J, Arganda-Carreras I, Frise E, Kaynig V, Longair M, Pietzsch T, et al. Fiji: an open-open source platform for biological-image analysis. Nat Methods 2012;9(7):676-82.

26 Clark RA, Shoaib M, Hewitt KN, Stanford SC, Bate ST. A comparison of InVivoStat with other statistical software packages for analysis of data generated from animal experiments. J Psychopharmacology 2012;26(8):1136-42.

27 Engler AG, Sen S, Sweeney HL, Discher DE. Matrix elasticity directs stem cell lineage specification. Cell 2006;126(4):677-89.

28 Cho JS, Yoo DS, Chung YC, Rhee SH. Enhanced bioactivity and osteoconductivity of hydroxyapatite through chloride substitution. J Biomed Mater Res A 2014;102(2):455-69.

29 Kanou M, Ueno T, Kagawa T, Fujii T, Sakata Y, Ishida N et al. Osteogenic Potential of Primed Periosteum Graft in the Rat Calvarial Model. Annals of Plastic Surgery 2005;54(1):71-8.

30 Umoh JU, Sampaio AV, Welch I, Pitelka V, Goldberg HA, Underhill TM et al. *In vivo* micro-CT analysis of bone remodeling in a rat calvarial defect model. Phys Med Biol 2009;54:2147-61.

31 Schmitz JP, Hollinger JO. The critical size defect as an experimental model for craniomandibulofacial nonunions. Clin Orthop 1986;205:299-308.

32 Bosch C, Melsen B, Vargervik K. Importance of the Critical-Size Bone Defect in Testing Bone-Regeneration Materials. J Craniof Surg 1998;9(4):310-6.

33 Lambers FM, Kuhn G, Müller R. Advances in multimodality molecular imaging of bone structure and function. BoneKEy Reports 1 2012;Article number 37:1-8.

34 Ventura M, Boerman OC, de Korte C, Rijpkema M, Heerschap A, Oosterwijlk, et al. Preclinical Imaging in Bone Tissue Engineering. Tissue Engineering: Part B 2014;00(00):1-17.

35 Koort JK, Mäkinen TJ, Knuuti J, Jalava J, Aro HT. Comparative ^{18}F-FDG PET of Experimental *Staphylococcus aureus* Osteomyelitis and Normal Bone Healing. J Nucl Med 2004;45:1406-11.

36 Ullm S, Krüger A, Tondera C, Gebauer TP, Neffe AT, Lendlein A, et al. Biocompatibility and inflammatory response *in vitro* and *in vivo* to gelatin-based biomaterials with tailorable elastic properties. Biomaterials 2014;35:9755-66.

37 Zitzmann NU, Schärer P, Marinello CP. Long-term results of implants treated with guided bone regeneration: a 5-year prospective study. Int J Oral and Maxillofac Implants 2001;16(3)355-66.

38 Brandt J, Bierögel C, Holweg K, Hein W, Grellmann W. Extended push-out test to characterize the failure of bone-implant interface. Biomed. Technik 2005;50(6):201-6.

39 Nelson TJ, Behfar A, Terzic A. Strategies for Therapeutic Repair: The "R^3" Regenerative Medicine Paradigm. Clin Transl Sci 2008;1(2):168-71.

40 Lee K, Silva EA, Mooney DJ. Growth factor delivery-based tissue engineering: general approaches and a review of recent developments. J R Soc Interface 2011;8:153-70.

41 Porter JR, Ruckh TT, Popat KC. Bone Tissue Engineering: A Review in Bone Biomimetics and Drug Delivery Strategies. Biotechnol Prog 2009;25(6):1539-60.

42 Maheshwari G, Brown G, Lauffenburger DA, Wells A, Griffith LG. Cell adhesion and motility depend on nanoscale RGD clustering. J Cell Sci 2000;113(Pt 10):1677-86.